RSC Advances

PAPER

View Article Online
View Journal | View Issue



Cite this: *RSC Adv.*, 2021, **11**, 8290

# Degradation of textile dyes from aqueous solution using tea-polyphenol/Fe loaded waste silk fabrics as Fenton-like catalysts

Md Shipan Mia,[a] Ping Yao,[b] Xiaowei Zhu,[a] Xue Lei,[a] Tieling Xing *[a] and Guoqiang Chen[a]

In this study, waste silk fabrics (SF) were modified with tea-polyphenols (TPs) and then iron ($Fe^{2+}$). The modified silk fabrics (TP-SF/Fe) were characterized *via* Fourier-transform infrared (FTIR), energy dispersive spectroscopy (EDS), scanning electron microscopy (SEM), and X-ray photoelectron spectroscopy (XPS) analysis. TP-SF/Fe was used in the Fenton-like removal of dyes (methylene blue, reactive orange GRN, and cationic violet X-5BLN) from aqueous solutions with catalyst-like activity. The effects of different catalyst samples, contact time, $H_2O_2$ concentration, initial dye concentration, and pH values on dye removal were investigated. The results showed that the dye removal percentages with the TP-SF/Fe-$H_2O_2$ sample reached 98%, 97%, and 95% in 5–40 min for methylene blue, reactive orange GRN, and cationic violet X-5BLN, respectively. Different thermodynamic and kinetic models were used to check the best fit of the adsorption data. The results indicated that the Freundlich isotherm and pseudo first-order kinetics models were the best fits. Moreover, it was also proved that TP-SF/Fe would be quite an effective and economical adsorbent for the treatment of textile dye wastewater. This work provides the basis for waste silk application in the removal of dyes from wastewater.

Received 22nd December 2020
Accepted 8th February 2021

DOI: 10.1039/d0ra10727a

rsc.li/rsc-advances



## 1. Introduction

Dyeing wastewater from the textile industries produces highly polluted effluents and is a serious concern for the environment and human beings.[1–3] Approximately ten thousand different dyes are currently used in the textile industries and the amount of wastewater is huge.[4,5] Compared with natural dyes, the dyeing wastewater from synthetic dyes rapidly increases pollution levels because of their low synthesis cost,[6] high toxicity,[7] good chemical stability,[8,9] strong bioaccumulation and color diversity. They have strong resistance to conventional treatment methods[10–12] and sunlight and they cause serious damage to aquatic life when discharged into water.[13,14] Dye wastewater causes many human diseases such as lung cancer, skin irritation, allergy, heart disease, chromosomal aberrations, kidney and liver damage, and respiratory diseases.[15–18] Therefore, it is necessary to remove these dyes from wastewater before it is discharged into the water system.

In recent years, researchers have developed various methods and techniques to remove toxic pollutants from the wastewater of textile industries.[19–22] Among those efforts, various techniques have been considered to remove dyes from wastewater such as coagulation, adsorption, membrane filtration, biological processes, microextraction, photocatalysis, Fenton-like removal and electrochemical methods.[23–26] Among these technologies, Fenton-like removal technology has attracted wide attention due to its high degradation capability, low cost and environmental friendliness although the reaction mostly requires $H_2O_2$ and Fenton or Fenton-like reagents. In addition, during the treatment process, the Fenton or Fenton-like reaction directly breaks down dye molecules without post-processing.[27,28]

Currently, the Fenton process is attracting more interest for the degradation of dyes.[29,30] In this process, hydroxyl radicals ($^{\bullet}OH$) are produced, which are highly reactive and powerful oxidants capable of degrading organic and inorganic compounds into water.[31,32] However, the homogeneous Fenton process also has some drawbacks from the perspective of practical application and this system has some limitations such as acidic pH conditions, a huge amount of final sludge, time-consuming processes and high cost.[33,34] Immobilization of iron particles (Fe) may be a suitable and stable remediation technique to overcome these limitations. The immobilization of iron has garnered a great deal of interest in the prevention of secondary water pollution due to its potential for having lower costs, higher reactivity and wider uses compared to other treatments.[35,36] However, this research was inspired by our previous study on immobilizing the iron (Fe) particles of a Fenton-like removal process on activated silk fiber for heterogeneous catalytic applications.[37]

[a]*National Engineering Laboratory for Modern Silk, College of Textile and Clothing Engineering, Soochow University, No. 199, Renai Road, Suzhou 215123, China. E-mail: xingtieling@suda.edu.cn*

[b]*Suzhou Institute of Trade and Commerce, Suzhou 215009, China*

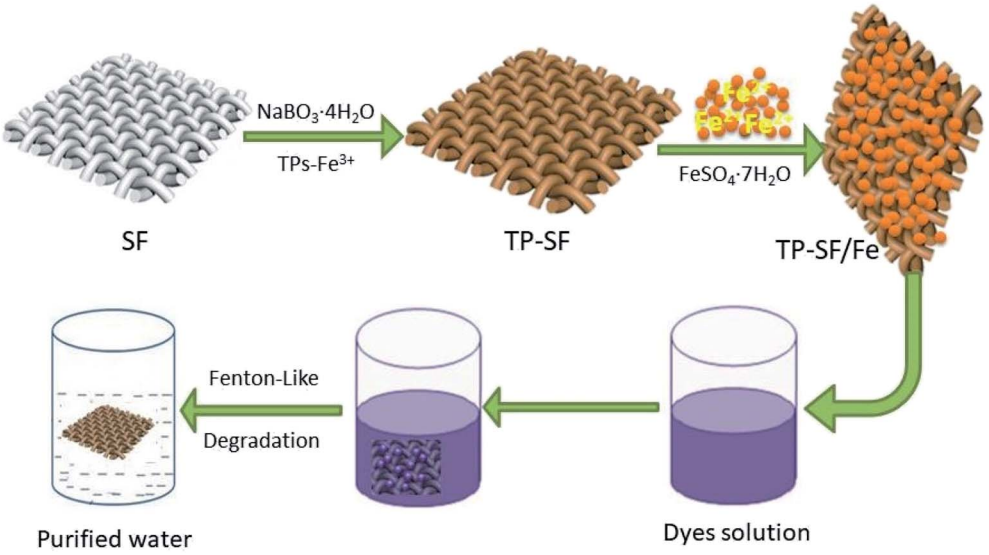


Fig. 1 A schematic diagram of TP-SF/Fe preparation and its adsorption of dyes.

Silk is a standard natural fibrous protein fiber widely used in textiles and biomedical applications due to its slow degradation, excellent biocompatibility and mechanical properties.[38–40] Moreover, silk is more extensively used in the textile industries to meet consumer demands and at the same time, lots of fabric is wasted in the processes.[41,42] Waste silk fabric samples that cannot be used for any other purpose are a worldwide concern. An alternative use of waste silk fabric provided through this work could be a sustainable remedy.

Polyphenol is a very effective component and can be used for different purposes. The structure of polyphenol compounds is considered to have an effective influence on improving the surface reactivity of hydrophobic and hydrophilic surfaces as well as other functional groups.[43–45] Tea is a compound widely used in the world and tea leaves are rich in natural polyphenolic compounds. Tea polyphenols (TPs) are used in beverage and food industries, as well as being investigated in health, biological and medicine services.[46,47] Tea polyphenols are also used in textile industries for coloration.[48,49] However, TPs are extensively used in dye adsorption, heavy metal adsorption, antibacterial, antimicrobial, UV protective and super-hydrophobic fields due to their strong functional properties.[50–52] The properties of TPs are similar to dopamine, but their cost is relatively low. Thus, TPs can be used as effective components in the coloration and functional modification of textiles.

In this present work, waste silk fabric was coated using TPs by rapid oxidative polymerization and iron particles ($Fe^{2+}$) were effectively immobilized onto the fabric surface, which was used for the Fenton-like degradation of methylene blue, reactive orange GRN and cationic violet X-5BLN dyes from aqueous solution, as shown in Fig. 1. The TPs grafted iron-loaded silk fabric (TP-SF/Fe) was characterized by using several instrumental techniques such as SEM and XPS. Moreover, the degradation process was investigated by various parameters, including different catalyst samples, contact time, $H_2O_2$ concentration, initial dye concentration and pH values. The isotherm and kinetics models of dye degradation were also analyzed.

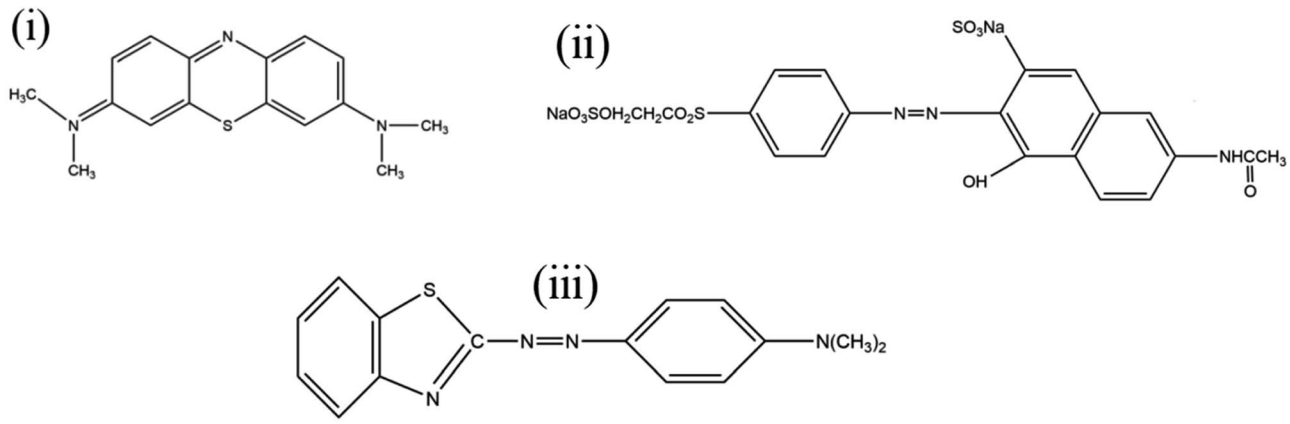


Fig. 2 The chemical structure of (i) methylene blue, (ii) reactive orange GRN, and (iii) cationic violet X-5BLN dyes.

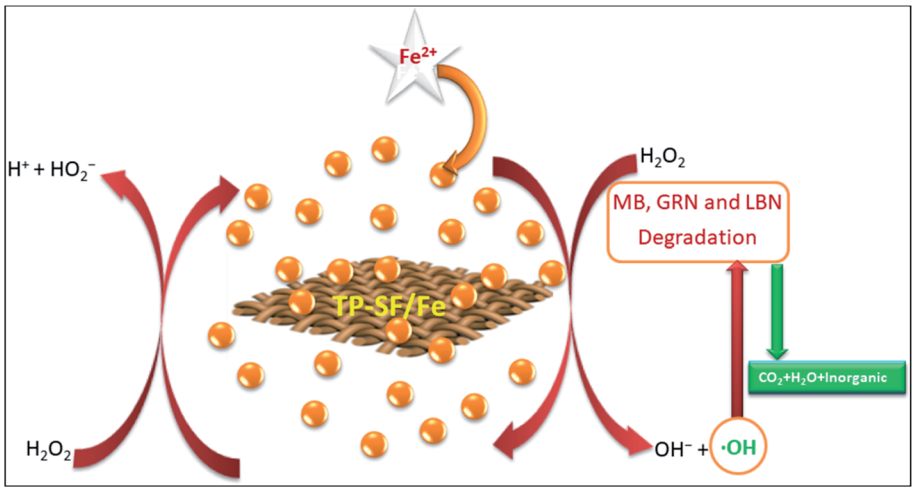


Fig. 3 A schematic diagram of the postulated mechanism of the degradation of the dyes.

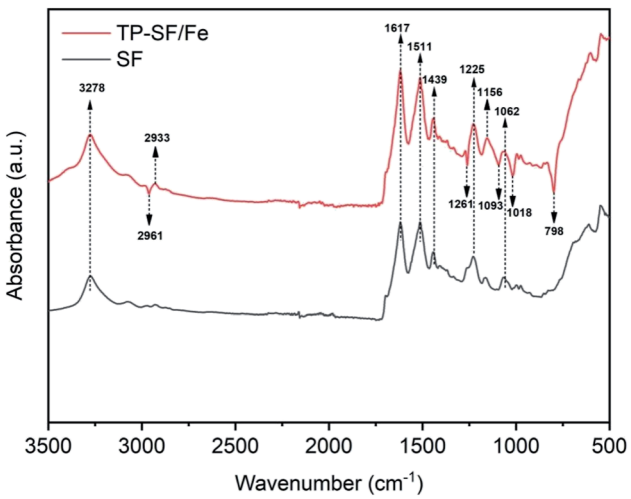


Fig. 4 Infrared spectra of untreated and treated silk.

# 2. Materials and methods

## 2.1 Materials

In this study, waste silk fabric (48 g $m^{-2}$) was provided by Huzhou Jiangnan Hengsheng Refining and Dyeing Co., Ltd. (China). Tea polyphenols (TPs) (purity 98.5%) were purchased from Shanghai Yuanye Biotechnology Co. Analytical grade sodium perborate ($NaBO_3 \cdot 4H_2O$), ferric chloride hexahydrate ($FeCl_3 \cdot 6H_2O$), hydrogen peroxide ($H_2O_2$, 33%), and ferrous sulfate heptahydrate ($FeSO_4 \cdot 7H_2O$) were obtained from Shanghai Lingfeng Chemical Reagent Co., Ltd. (Shanghai, China). Methylene blue (MB), reactive orange GRN (GRN) and cationic violet X-5BLN (BLN) dyes were purchased from Tianjin Tianshun Chemical Dyestuff Co., Ltd (Tianjin, China).

## 2.2 Preparation of the functional silk fabrics

In this work, silk fabric (15 × 15 $cm^2$) was immersed in 150 mL of deionized water containing 2 g $L^{-1}$ tea polyphenol and 2 mmol $L^{-1}$ ferric chlorides ($FeCl_3 \cdot 6H_2O$) and placed in a shaking water bath for 20 min at 50 °C. Then 12 mmol $L^{-1}$ of sodium perborate ($NaBO_3 \cdot 4H_2O$) was added and the final solution was stirred for 40 min. The resultant coated silk fabric (TP-SF) was removed and rinsed using deionized water then dried in air. Afterward, the coated dried silk fabric was directly put into 1400 mL deionized water containing 40 mmol $L^{-1}$ $FeSO_4 \cdot 7H_2O$ for 24 h at room temperature. Finally, the TP-SF/Fe sample was taken out and rinsed with deionized water and dried overnight in ambient condition. The chemical structure of the three dyes (cationic blue, anionic orange and cationic based violet dyes) are shown in Fig. 2.

## 2.3 Characterization of TP-SF/Fe

Fourier transform infrared (FTIR) spectroscopy of TP-SF/Fe was performed using a Nicolet-5700 Fourier transform infrared spectrometer in the range of 400–4000 $cm^{-1}$. The surface morphology of silk fabric was analyzed by scanning electron microscopy (SEM,

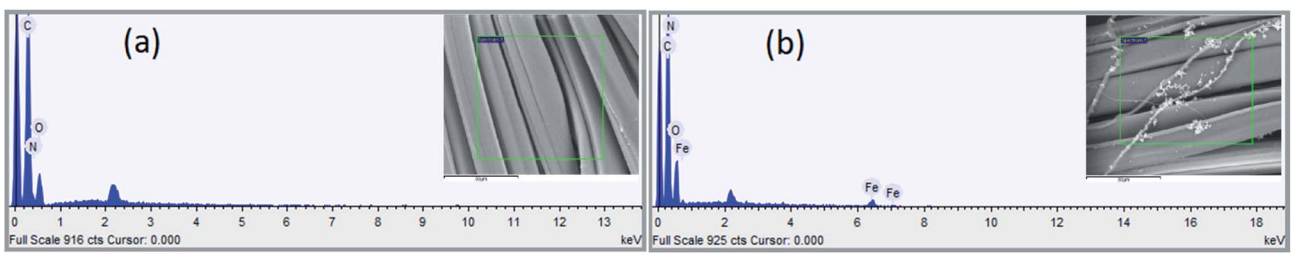


Fig. 5 Energy dispersive spectra of (a) SF and (b) TP-SF/Fe.

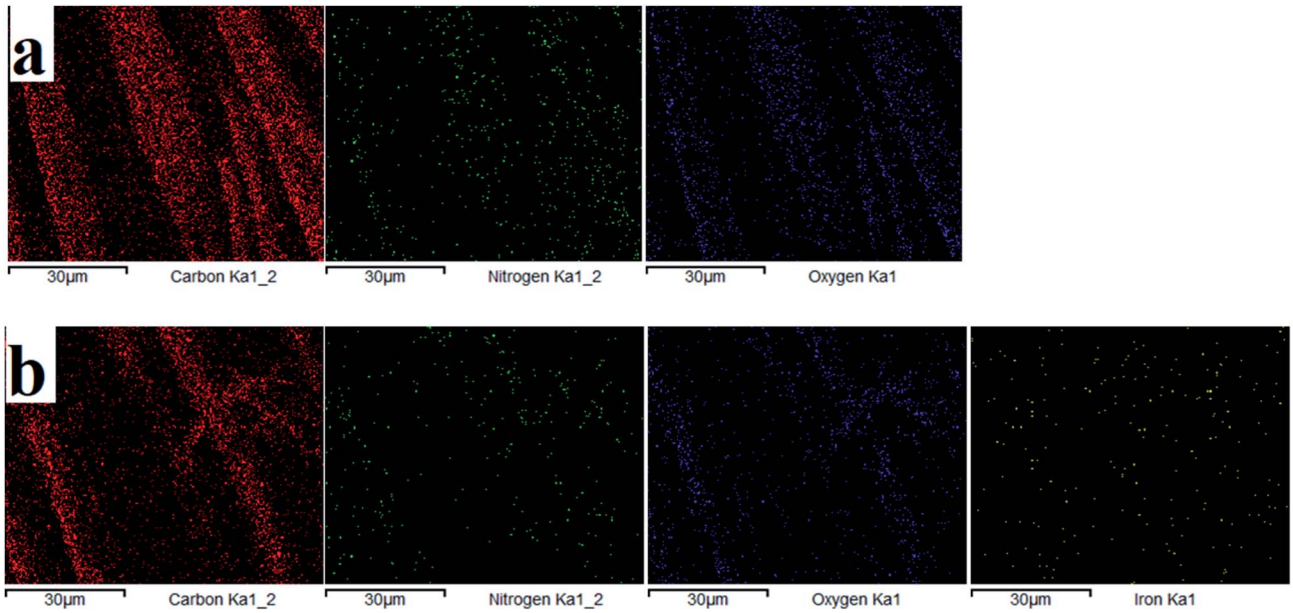


Fig. 6 Energy dispersive spectra of (a) SF and (b) TP-SF/Fe with different element mapping images.

Hitachi S-4800). The elemental detection of the silk fabric and its percentage atomic weight was carried out by energy dispersive X-ray spectroscopy (EDS) using BRUKNER axes EDS analyzer mounted with SEM. The surface elements of TP-SF/Fe were verified by X-ray photoelectron spectra (XPS) through a Thermo ESCALAB 250XI spectrometer (Thermo Fisher Scientific, USA) using an Al Kα X-ray source (1484.6 eV). The degradation of TP-SF/Fe was measured using a double beam UV-Vis spectrophotometer (Hitachi UH-4150) in the wavelength range 300–800 nm at room temperature.

### 2.4 Dye degradation procedure and analysis

The TP-SF/Fe was evaluated by the heterogeneous Fenton-like removal of (methylene blue, reactive orange GRN and cationic

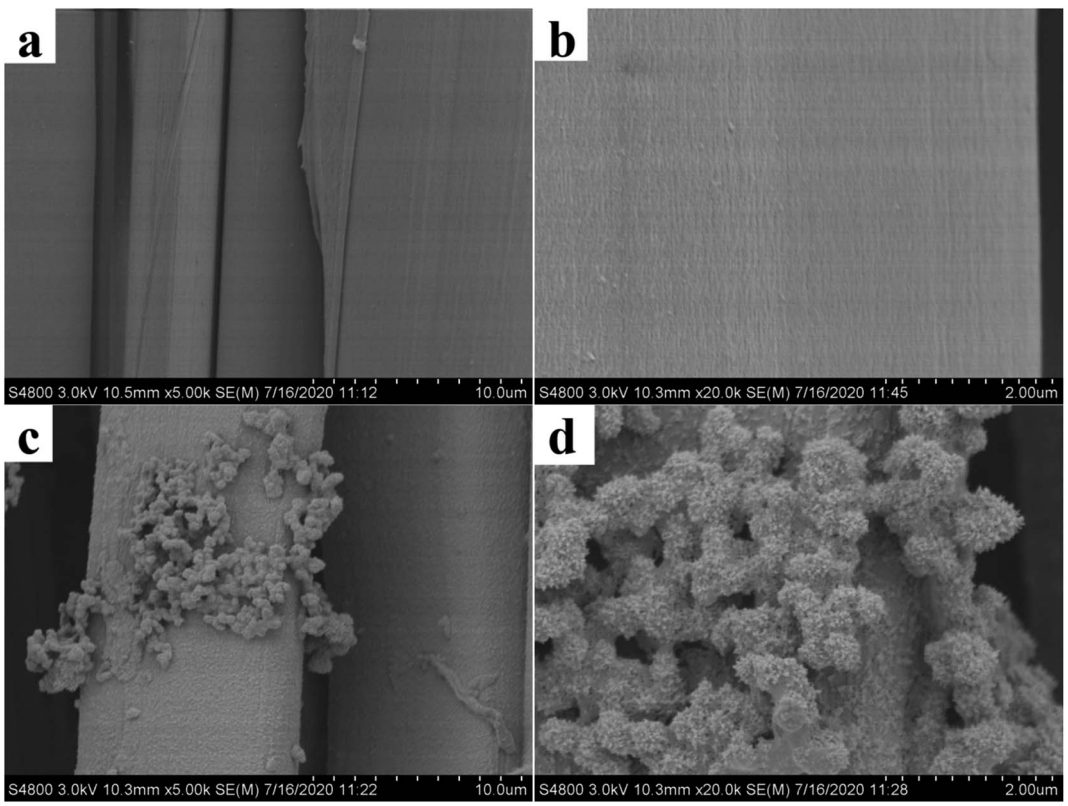


Fig. 7 SEM images of SF (a, b) and TP-SF/Fe (c, d) at different magnifications

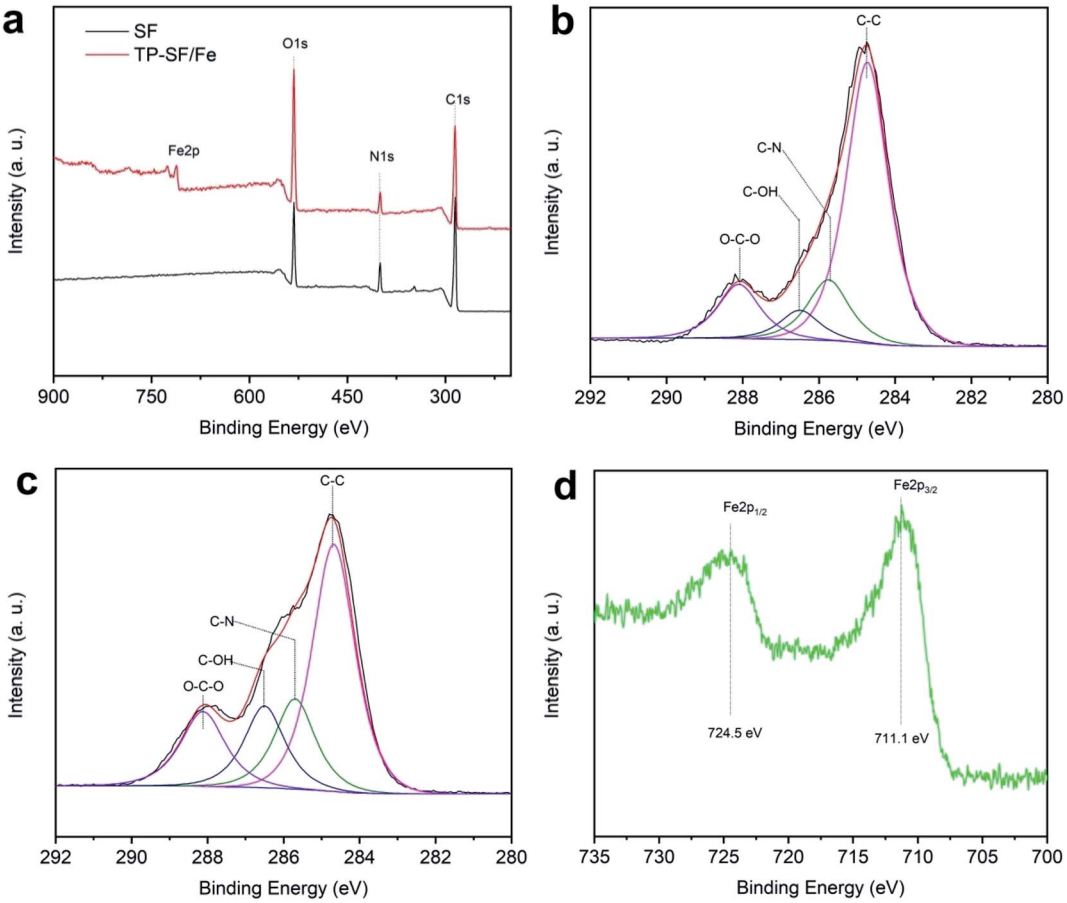


Fig. 8 (a) Wide-scan XPS spectra of the silk fabrics, high-resolution C 1s spectra of (b) SF and (c) TP-SF/Fe, and (d) the core-level Fe 2p spectrum of TP-SF/Fe.

violet X-5BLN) dyes in the presence of hydrogen peroxide ($H_2O_2$). In the rotatory shaker, 0.1 g TP-SF/Fe (adsorbent) was added into 70 mL aqueous solution with 20 mg $L^{-1}$ of dyes for 40 min at 50 °C with stirring. In this experiment, the concentrations of dyes in the solutions were measured every 5 min until degradation was complete and the remaining amount of dyes in the aqueous solution was determined by UV-spectrophotometer. The dye removal percentage ($R$) and removal capacity ($q_e$) was calculated using the following equations:

$$q_e = \frac{V(C_0 - C_e)}{m} \quad (1)$$

$$R\% = \frac{(C_0 - C_e)}{C_0} \times 100 \quad (2)$$

Table 1 Surface elemental compositions (atomic weight percentage) of silk fabric samples

| | Sample (%) | |
|---|---|---|
| Surface element | SF | TP-SF/Fe |
| N | 10.94 | 6.41 |
| O | 17.84 | 29.95 |
| C | 70.75 | 61.02 |
| Fe | 0.46 | 2.62 |

where $C_0$ is the initial concentration of dye and $C_e$ is the concentration of dyes at different time intervals, $q_e$ (mg $g^{-1}$) is the amount of dye removal capacity, $V$ (L) is the volume of the solution and $m$ (g) is the mass of adsorbent. The maximum absorption wavelength of the dye in the visible region was calculated by $C/C_0$ at $\lambda_{max}$: (664, 591 and 475 nm for methylene blue, reactive orange GRN and cationic violet X-5BLN). Dye removal is influenced by different factors such as the effect of contact time (5 to 40 min), $H_2O_2$ concentration (0.01 to 5 mmol $L^{-1}$), dye concentration (10 to 80 mg $L^{-1}$) and pH (3 to 11). The pH was adjusted by using 0.1 mol $L^{-1}$ $HNO_3$ and 0.1 mol $L^{-1}$ NaOH solutions.

### 2.5 Degradation mechanism

Based on the results described in the section above, the proposed mechanism of MB, GRN and BLN dye degradation by TP-SF/Fe is presented in Fig. 3. Ferrous ions can be mineralized into FeOOH by TP-SF like PDA-SF.[53] The TP-SF/Fe-$H_2O_2$ catalyst can efficiently degrade dyes due to the presence of hydroxyl ions on the surface of TPs. The TP-SF/Fe-$H_2O_2$ was considered for the Fenton-like reaction in the presence of $H_2O_2$ which can catalyze the production of hydroxyl $^{\bullet}OH$ radicals from $H_2O_2$.[54,55] The hydroxyl $^{\bullet}OH$ radicals can break the existing azo bond in dye molecules, thus destroying the structure of dyes.

The postulated reaction mechanism is shown in the three following steps:

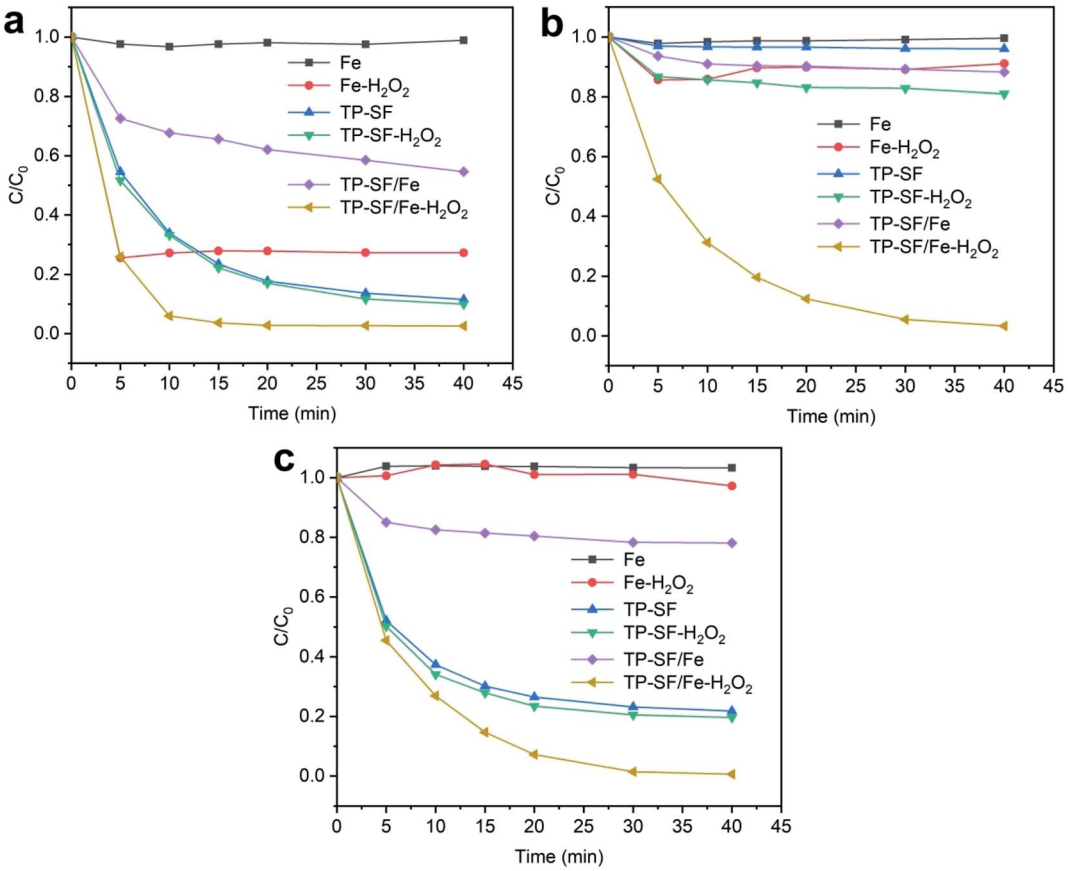


Fig. 9 Evolution over time of $C/C_0$ for different catalyst samples in three dye solutions: (a) methylene blue, (b) reactive orange GRN, and (c) cationic violet X-5BLN (sample: 0.1 g, $H_2O_2$ concentration: 0.1 mmol $L^{-1}$, dye concentration: 20 mg $L^{-1}$, time: 40 min, and $T$: 50 °C).

(i) The process of producing the reactive species

$$Fe^{2+} + \text{TP-SF} \rightarrow \text{TP-SF/Fe (FeOOH)}$$

$$FeOOH + H_2O_2 \rightarrow FeOO^- + {}^{\bullet}OH + H_2O$$

(ii) The process of color removal of the dyes

$$\text{Dyes} + {}^{\bullet}OH \rightarrow \text{reaction intermediates}$$

(iii) The process of mineralization

$$\text{Reaction intermediates} + {}^{\bullet}OH \rightarrow CO_2 + H_2O + \text{inorganics}$$

# 3. Results and discussion

## 3.1 Characterization

**3.1.1 FTIR analysis.** To determine the presence of active molecules in the stabilization of $Fe^{2+}$ ions in SF, Fourier transform infrared spectroscopy (FTIR) of SF and TP-SF/Fe was conducted. It can be observed from Fig. 4 that the absorption peaks appearing at 3278, 2961 and 2933 $cm^{-1}$ were attributed to the –OH and C–H stretching vibration belonging to polyphenols present in waste silk, respectively.[56,57] The band at 1617 $cm^{-1}$ was attributed to the stretching vibration of –C=O indicating bending of the untreated and treated waste silk fabric. The band peaks appearing at 1511, 1439, 1225 and 1062 $cm^{-1}$ represented the bending vibrations of N–H, C–N, O–H and C–O–C, respectively.[52] Moreover, the FT-IR spectra of TP-SF/Fe with band peaks at 1261, 1156, 1093, 1018 and 798 $cm^{-1}$ indicated the formation of Fe–O due to the presence of TPs which confirms the loading of the iron particles.

**3.1.2 EDS analysis.** The elemental composition on the fiber surface before and after treatment was evaluated using EDS analysis (see Fig. 5 and 6). The major elements of C, N, and O were observed in the EDS spectra. It is obvious from the EDS spectra and maps that there are different surface element compositions on the treated and untreated samples. After loading of iron, the EDS spectrum showed the peak intensity of the Fe element confirming the formation of TP-SF/Fe. Fig. 6(b) shows the iron element of TP-SF/Fe, which is derived from the presence of some Fe-oxides in tea-phenols.

**3.1.3 SEM analysis.** The surface morphology of the waste silk before and after modification was investigated through SEM analysis as shown in Fig. 7. It is clear from the SEM pictures that the surface of the SF is very smooth as shown in Fig. 7(a) and (b). Conversely, the SEM image of the surface of TP-SF/Fe was more rough (Fig. 7(c) and (d)), indicating that the

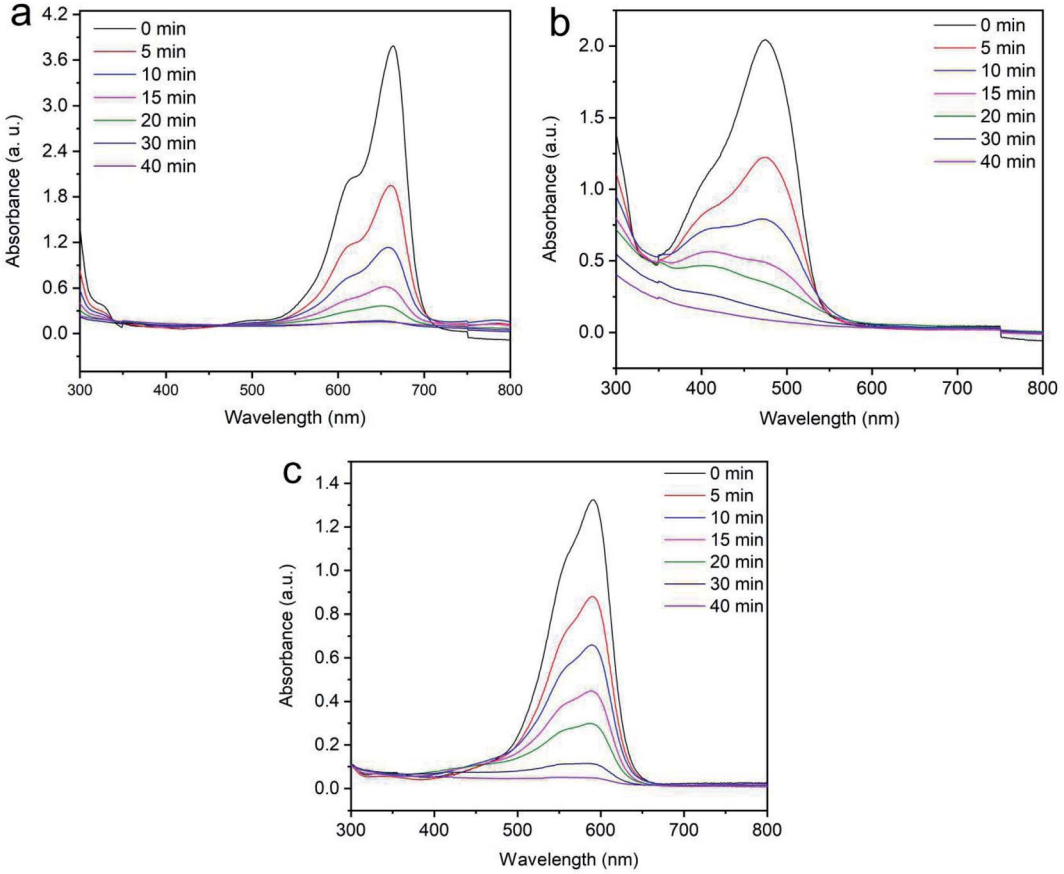


Fig. 10 UV-visible spectral changes for the degradation of dyes: (a) methylene blue, (b) reactive orange GRN, and (c) cationic violet X-5BLN dye degradation as a function of time (TP-SF/Fe = 0.1 g, dye concentration = 20 mg $L^{-1}$, $H_2O_2$ concentration = 1.0 mmol $L^{-1}$, and $T$ = 50 °C).

modified silk fabric is successfully covered by the tea-phenols/Fe coating.[58,59] However, it can be considered that the presence of functional groups on the surface of tea-phenols/Fe silk fabric could be chosen as a research model for further studies.

**3.1.4 XPS analysis.** X-ray photoelectron spectroscopy (XPS) was performed to compare and verify the oxidation states of elements present on the surface of the fabric before and after treatment as shown in Fig. 8(a)–(d) and Table 1. It can be seen from Fig. 8(a) that C, N, and O element peaks appear in the XPS spectrum of SF and TP-SF/Fe samples, but a peak corresponding to the iron (Fe) element appears on the surface spectrum of TP-SF-Fe. In addition, Fig. 8(b) and (c) display the C 1s spectra of the surface of the SF and TP-SF/Fe samples, and the C 1s XPS spectra are fitted to the absorption peaks at 284.7, 285.7, 286.5 and 288.1 eV, corresponding to the C–C, C–N, C–OH, and O–C O bonds, respectively.[60–62] Furthermore, Fig. 8(d) shows the core-level Fe 2p on the surface of the TP-SF-Fe, and the characteristic peaks are attributed to Fe $2p_{3/2}$ (711.1 eV) and Fe $2p_{1/2}$ (724.5 eV), respectively. Therefore, the XPS results indicated that iron mineralization on the tea-phenol coated silk fibers existed in the oxidation state.

### 3.2 Factors influencing the removal of dyes from aqueous solution

**3.2.1 The effect of different catalyst systems.** The effect of different samples for adsorption of methylene blue, reactive orange GRN, and cationic violet X-5BLN dyes was evaluated for the Fe, Fe-$H_2O_2$, TP-SF, TP-SF-$H_2O_2$, TP-SF/Fe, and TP-SF/Fe-$H_2O_2$ samples, in which the same amount of $Fe^{2+}$ or TP was applied. Fig. 9 shows that TP-SF/Fe-$H_2O_2$ is the most effective at degrading dyes and the highest efficiency is about 98% for methylene blue, 99% for reactive orange GRN, and 96% for cationic violet X-5BLN dyes. The TP-SF and TP-SF-$H_2O_2$ dye removal rate is lower and could not meet the requirements. In addition, the dye removal efficiency for Fe and Fe-$H_2O_2$ is much lower and does not show sufficient change. High efficiency removal of dyes can be obtained with a high dosage of $H_2O_2$ in the traditional Fenton reaction. It can be seen from Fig. 9 that TP-SF/Fe resulted in a lower degradation rate; on the other hand, TP-SF/Fe with a small amount of $H_2O_2$ (0.1 mmol $L^{-1}$) generated a strong reaction system, which effectively increased the release rate of hydroxyl radicals and degraded most of the dyes in a short time. This signifies that the TP-SF/Fe-$H_2O_2$ samples are stable and can be used for dye degradation experiments.

**3.2.2 Effects of contact time for the degradation of dyes.** The function of contact time on dye removal is a vital factor for cost minimization in industrial usage. In this work, Fenton-like degradation of aromatic dyes (methylene blue, reactive orange GRN and cationic violet X-5BLN) was carried out with different contact times and analyzed by UV-Vis spectrophotometry. The

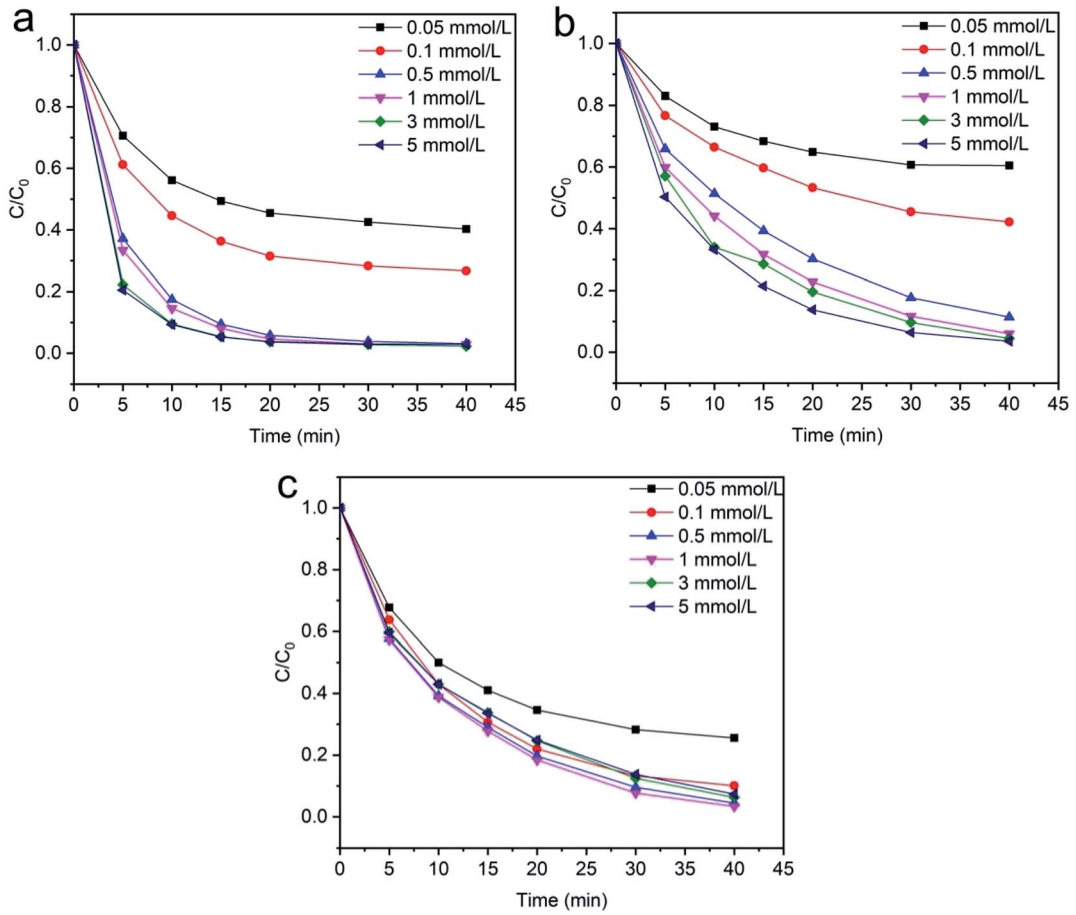


Fig. 11 Evolution over time of $C/C_0$ for the degradation of dye: (a) methylene blue, (b) reactive orange GRN, and (c) cationic violet X-5BLN dye degradation as a function of $H_2O_2$ concentration (TP-SF/Fe = 0.1 g, dye concentration = 20 mg $L^{-1}$, time = 40 min, $T$ = 50 °C).

Fenton-like reaction was constructed with iron loaded silk and hydrogen peroxide ($H_2O_2$) for degrading organic pollutants. As shown in Fig. 10(a)–(c), the contact time for the dye removal process was kept at 40 min to optimize the adsorption uptake with 0.1 g of sample, initial dye concentration of 20 mg $L^{-1}$ and at 50 °C. It can be seen from Fig. 10(a) that the MB dye exhibits the maximum absorption peak intensity at 664 nm observed with the function of the reaction time and after 40 minutes the most degradation is achieved.[63] Furthermore, Fig. 10(b) and (c) shows that the reactive orange GRN and cationic violet X-5BLN dyes exhibit the maximum absorption peak intensity at 591 nm and 475 nm after 40 min of stirring, respectively.[64–66] It can be concluded that Fenton-like removal experiments using TP-SF/Fe can reach sufficient degradation effects within 40 min.

**3.2.3 Effects of $H_2O_2$ concentration.** The degradation of (methylene blue, reactive orange GRN and cationic violet X-5BLN) dyes were carried out using different concentrations of $H_2O_2$ (0.05, 0.1, 0.5, 1, 3, and 5 mmol $L^{-1}$) and the results are illustrated in Fig. 11(a)–(c). The dye removal capacity was evaluated by the terms of $C/C_0$ after reaction with different doses of $H_2O_2$. Fig. 11 shows that, with an increase in $H_2O_2$ dose from 0.5 to 5 mmol $L^{-1}$, the dye removal efficiency increased respectively within 40 min of reaction due to the enhanced production of hydroxyl radicals, and when the dose of $H_2O_2$ was 0.05 and 0.1 mmol $L^{-1}$, the dye degradation rate was insufficient. However, the dose of 1 mmol $L^{-1}$ of $H_2O_2$ was appropriate, and the maximum degradation efficiency was obtained within 40 min in comparison to the other high concentration doses. Furthermore, this phenomenon clearly indicated that high concentrations of $H_2O_2$ cannot increase the degradation efficiency.[67,68]

**3.2.4 Effects of initial dye concentration.** The wastewater from textile industries typically has a wide range of color concentration, which is extremely harmful to the environment. The effect of initial dye concentration on the degradation of methylene blue, reactive orange GRN and cationic violet X-5BLN dyes was investigated at different times from 5 to 40 min with an adsorbent dose of 0.1 g and $H_2O_2$ concentration of 1 mmol $L^{-1}$ at 50 °C. As shown in Fig. 12(a)–(c), different dye concentrations (10, 20, 40, 60 and 80 mg $L^{-1}$) are used to determine the effect of dye concentration on the removal of dyes. The results presented in Fig. 12(a) show that the maximum dye removal efficiency of the initial concentration from 10–20 mg $L^{-1}$ is obtained after reaction time at 40 min. As shown in Fig. 12(b) and (c), a similar character has been found in the other two dyes (reactive orange GRN and cationic violet X-5BLN) as a function of time.[60] However, it can be observed that as the concentration of the dye solution increases, the final degradation rate gradually reduces.

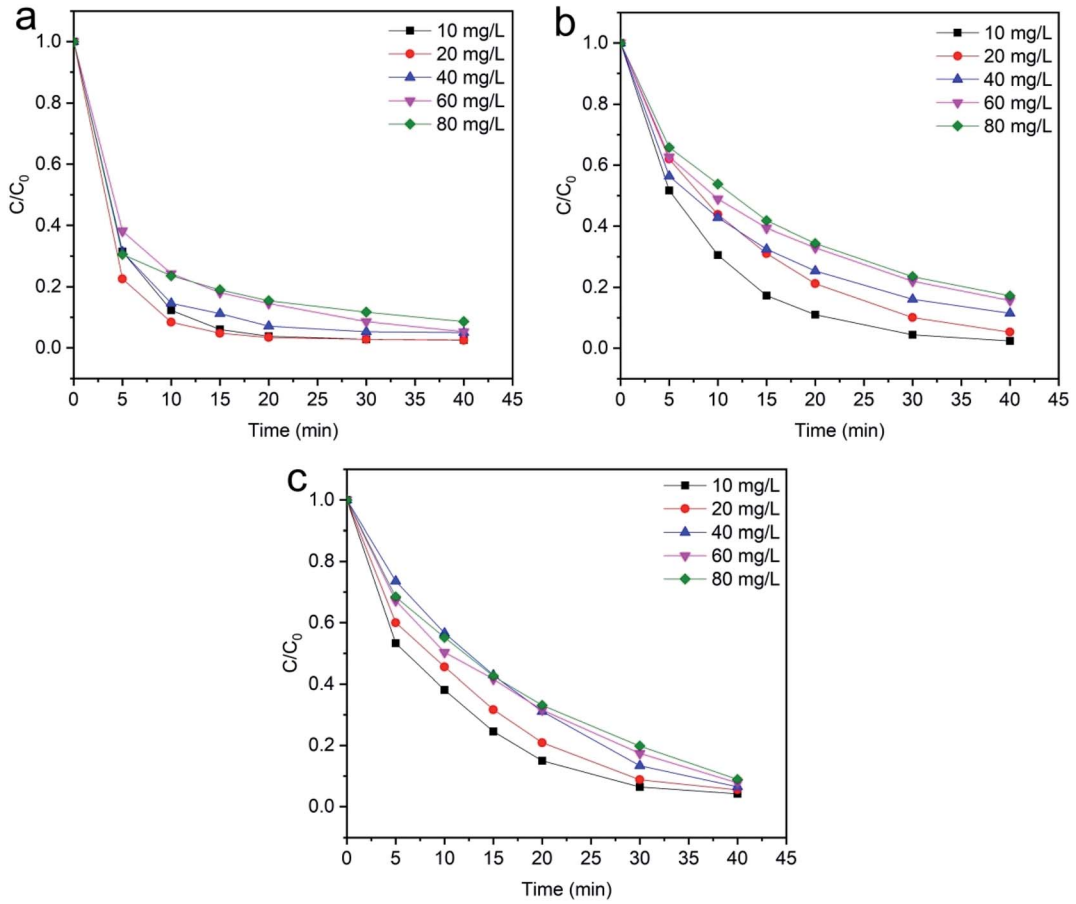


Fig. 12 Evolution over time of $C/C_0$ for the degradation of dyes: (a) methylene blue, (b) reactive orange GRN, and (c) cationic violet X-5BLN dye degradation as a function of dye concentration (TP-SF/Fe = 0.1 g, $H_2O_2$ concentration = 0.1 mmol $L^{-1}$, time = 40 min, and $T$ = 50 °C).

Although for a maximum dye concentration of 80 mg $L^{-1}$, the degradation efficiency was the lowest compared with other concentrations, but it still stayed over 91%, 83% and 91%, respectively. This phenomenon could be due to the fact that in the case of high dye concentration, the TP-SF/Fe catalyst can form a stable reaction system with $H_2O_2$. At this time, the hydroxyl radicals were not easy to neutralize, which increased the possibility of contact with the dyes and eventually led to a high removal.[69,70] These results suggested that a 20 mg $L^{-1}$ concentration could be the optimum dye concentration for the highest removal rate.

**3.2.5 Effects of pH.** The dyeing wastewater from the dyeing process of textiles has a wide range of pH values. The pH has an important role both in the characteristics of textile waste and the generation of hydroxyl radicals, which is greatly influenced in Fenton-like removal experiments by the surface of the catalyst.[71,72] The effect of the pH on the degradation experiments was investigated by using different pH values in the range of 3–10. The results obtained by the effect of pH on the degradation efficiency of dyes are shown in Fig. 13. The pH of the working solutions was maintained by using different amounts of 0.1 mol $L^{-1}$ NaOH and 0.1 mol $L^{-1}$ $HNO_3$. It is apparent from the results in Fig. 13(a) and (c) that the degradation efficiency is high in acidic and basic conditions and the degradation is most rapid at pH 3 and 11. In addition, Fig. 13(b) shows that the degradation efficiency gradually decreases at higher pH and most of the dyes are degraded at pH 3. Strong acidic conditions are conducive for the generation of hydroxyl radical groups, which favor dye degradation and also the characteristics of the Fenton reaction. However, under strong acidic conditions, the SF catalyst surface takes a negative charge and can adsorb more cationic dyes, which could explain the result of Fig. 13(a) and (c).

### 3.3 Theory of adsorption isotherms

The analysis of isotherms methods is an important way to accurately represent the relationship between adsorbent and adsorbate for methylene blue, reactive orange GRN and cationic violet X-5BLN. In this work, the models of Langmuir and Freundlich isotherms are applied to recognize the range and degree of favourability of adsorption.

**3.3.1 Langmuir isotherms.** The analysis is based on the Langmuir isotherm models, which assume a homogeneous surface with uniform adsorption energy and exclusive coverage of the adsorbent. The linearized form of the Langmuir isotherm model is expressed by the following eqn (3):

$$\frac{C_e}{q_e} = \frac{C_e}{q_m} + \frac{1}{K_L q_m} \quad (3)$$

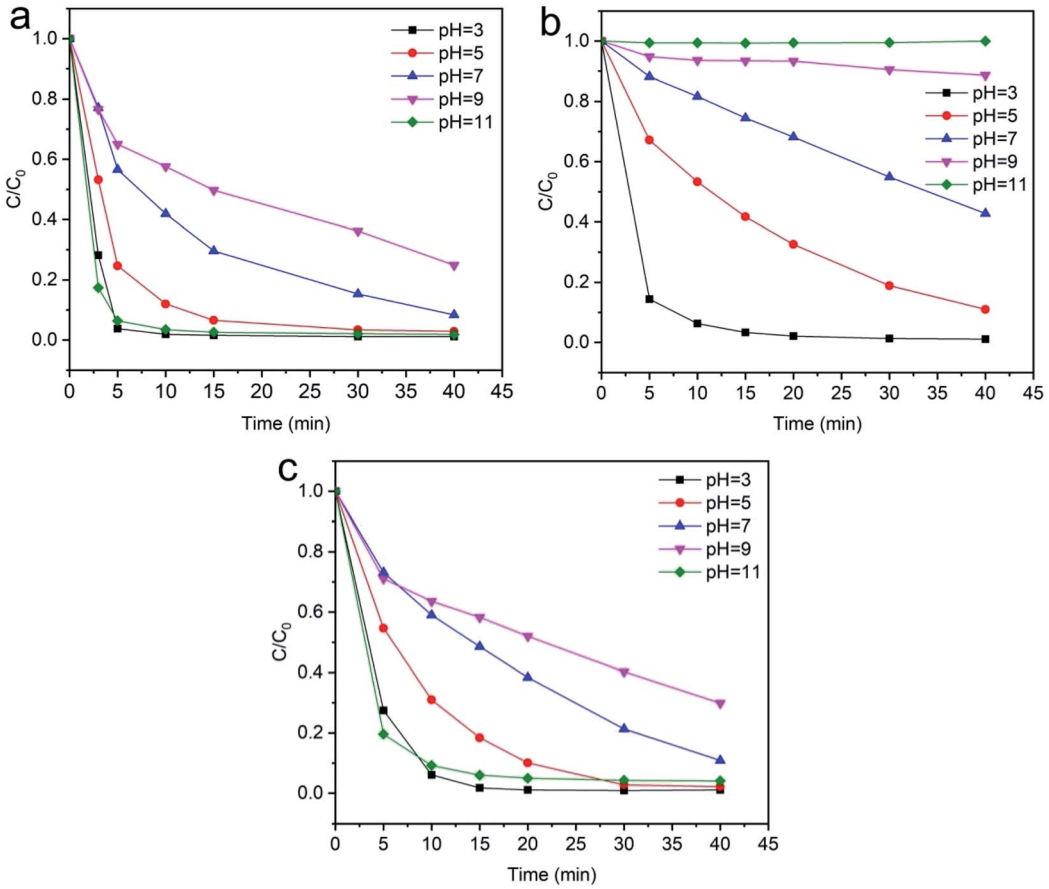


Fig. 13 Evolution over time of $C/C_0$ for the degradation of dyes: (a) methylene blue, (b) reactive orange GRN, and (c) cationic violet X-5BLN dye degradation as a function of pH (TP-SF/Fe = 0.1 g, $H_2O_2$ concentration = 0.1 mmol $L^{-1}$, dye concentration = 20 mg $L^{-1}$, time = 40 min, $T$ = 50 °C).

In this equation, $q_e$ (mg $g^{-1}$) is the absorbed amount of the dyes (methylene blue, reactive orange GRN and cationic violet X-5BLN) at equilibrium, $C_e$ (mg $L^{-1}$) is the equilibrium concentration of the dye solution, $K_L$ is the Langmuir constant connected to the free energy of adsorption, and $q_m$ (mg $g^{-1}$) is the maximum adsorption capacity at a complete monolayer.[73,74] The Langmuir isotherm parameters are determined from linear isotherm plots and the corresponding data are given in Fig. 14 and Table 2. The results obtained from the correlation coefficient ($R^2$ values) show that the Langmuir isotherm parameters are acceptable and fit for the dyes (methylene blue, reactive orange GRN and cationic violet X-5BLN) and the maximum adsorption capacity is 13.0993 mg $g^{-1}$ for the methylene blue dyes.

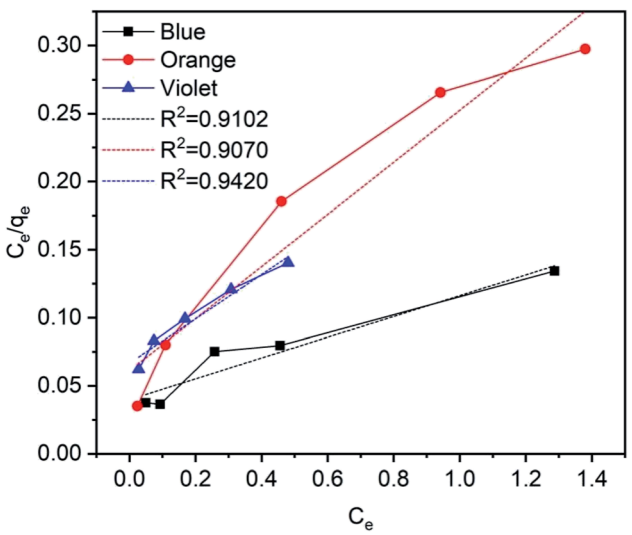


Fig. 14 Langmuir adsorption isotherms for methylene blue, reactive orange GRN, and cationic violet X-5BLN dyes.

**3.3.2 Freundlich isotherm.** The Freundlich model is applied to describe the adsorption of dye on a heterogeneous surface by multilayer adsorption. The linearized Freundlich isotherm adsorption model is exposed by eqn (4):

$$\log q_e = \left(\frac{1}{n}\right)\log C_e + \log K_f \quad (4)$$

where $q_e$ (mg $g^{-1}$) is the amount of dye adsorbed per unit weight of adsorbent, $n$ is the Freundlich constant indicative of

Table 2 Langmuir adsorption constants of dyes on TP-SF/Fe

| Type of dye | $q_m$ (mg $g^{-1}$) | $K_L$ | $R^2$ |
|---|---|---|---|
| Methylene blue | 13.0993 | 1.9131 | 0.91012 |
| Reactive orange GRN | 5.2260 | 3.1307 | 0.9070 |
| Cationic violet X-5BLN | 6.1376 | 2.4449 | 0.9420 |

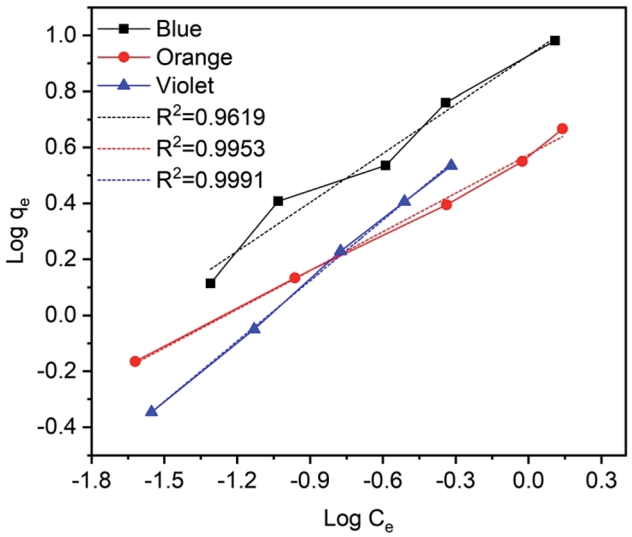


Fig. 15 Freundlich adsorption isotherms for methylene blue, reactive orange GRN, and cationic violet X-5BLN dyes.

Table 3 Freundlich adsorption constants of the dyes on TP-SF/Fe

| Type of dye | $n$ | $K_f$ | $R^2$ |
|---|---|---|---|
| Methylene blue | 1.714 | 2.5307 | 0.9619 |
| Reactive orange GRN | 2.1728 | 1.7759 | 0.9953 |
| Cationic violet X-5BLN | 1.3887 | 2.1644 | 0.9991 |

adsorption concentration of the adsorbents, and $K_f$ is the Freundlich coefficient related to the adsorption capacity of the dye adsorbed onto the adsorbent per unit equilibrium concentration. Freundlich parameters can be calculated and the values of $n$ and $K_f$ are achieved from the linear isotherm plots of log $q_e$ *versus* log $C_e$ curves[75,76] and their values are given in Fig. 15 and Table 3.

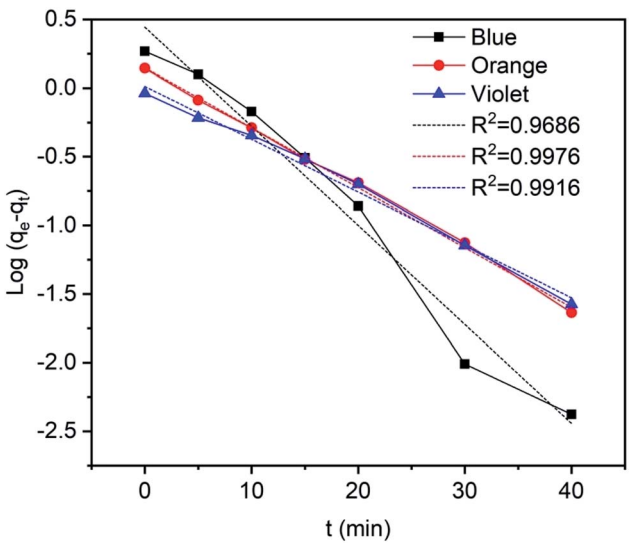


Fig. 16 Pseudo-first order kinetics for methylene blue, reactive orange GRN, and cationic violet X-5BLN dyes.

Table 4 Pseudo-first order kinetics parameters for methylene blue, reactive orange GRN, and cationic violet X-5BLN dyes on TP-SF/Fe

| Type of dye | $q_m$ (mg g$^{-1}$) | $k_1$ | $R^2$ |
|---|---|---|---|
| Methylene blue | 1.5582 | 0.07217 | 0.9686 |
| Reactive orange GRN | 1.159 | 0.04364 | 0.9976 |
| Cationic violet X-5BLN | 1.0122 | 0.0385 | 0.9916 |

Furthermore, the results indicate that the correlation coefficient values ($R^2$ values) are fitted for the methylene blue, reactive orange GRN and cationic violet X-5BLN dyes. This also suggests that dye removal on TP-SF/Fe may be multilayer coverage.

### 3.4 Adsorption kinetics

It is important to study the adsorption kinetics in dye removal from aqueous solutions. The kinetics of adsorption can be helpful to determine the adsorption capacity of dyes by TP-SF/Fe. The adsorption kinetics of methylene blue, reactive orange GRN and cationic violet X-5BLN dyes at different times were analyzed by applying pseudo-first order and pseudo-second order kinetic models to recognize the solute absorption rate and transient behavior of the adsorption process.

**3.4.1 Pseudo-first order kinetics.** The linearized form of pseudo-first order is given by eqn (5):

$$\ln(q_e - q_t) = \ln q_e - k_1 t \quad (5)$$

where $q_e$ (mg g$^{-1}$) is the equilibrium adsorption capacity, $q_t$ (mg g$^{-1}$) is the adsorption capacity at time $t$, and $k_1$ is the rate constant of the pseudo-first order model. The values of $k_1$ and adsorption capacity $q_e$ can be obtained from the slopes and intercepts of the plots of $\ln(q_e - q_t)$ against $t$, respectively. Moreover, the resultant parameters show that the correlation coefficient values of different dyes for the pseudo-first order

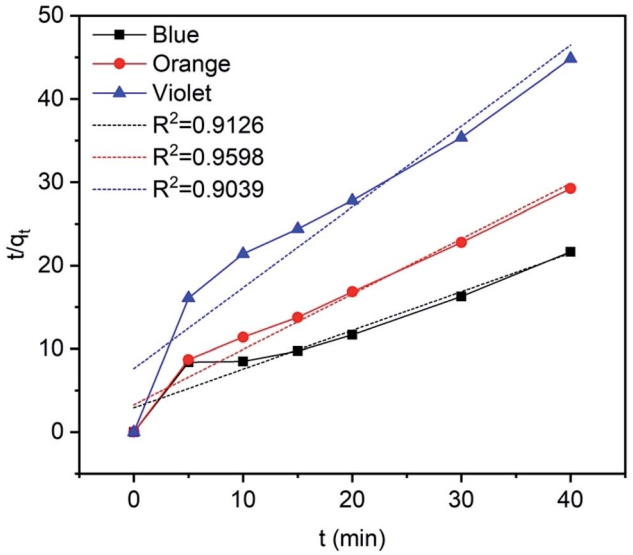


Fig. 17 Pseudo-second order kinetics for methylene blue, reactive orange GRN, and cationic violet X-5BLN dyes.

Table 5 Pseudo-second order kinetics parameters for methylene blue, reactive orange GRN, and cationic violet X-5BLN dyes on TP-SF/Fe

| Type of dye | $q_m$ (mg g$^{-1}$) | $k_2$ | $R^2$ |
|---|---|---|---|
| Methylene blue | 2.153 | 0.0738 | 0.9136 |
| Reactive orange GRN | 1.5049 | 0.1345 | 0.9598 |
| Cationic violet X-5BLN | 1.0299 | 0.1236 | 0.9039 |

model are acceptable and fitted (Fig. 16 and Table 4), indicating that pseudo-first order kinetics could be sufficient to describe the adsorption mechanism of dyes on the surface of TP-SF/Fe adsorbents.[77,78]

**3.4.2 Pseudo-second order kinetics.** The linearized form of pseudo-second order is given by eqn (6):

$$\frac{t}{q_t} = \left(\frac{1}{q_e}\right)t + \frac{1}{k_2 q_e^2} \quad (6)$$

where $q_e$ (mg g$^{-1}$) and $q_t$ (mg g$^{-1}$) is the adsorption capacity at time $t$ and at equilibrium, respectively and $k_2$ (g mg$^{-1}$ min$^{-1}$) is the pseudo-second order rate constant. The values of the pseudo-second order rate constant $k_2$ and equilibrium adsorption volume $q_e$ can be determined from the slopes and intercepts of the plots of $t/q_t$ *versus* $t$, respectively. The resultant parameter indicates that the correlation coefficient values of different dyes for the pseudo-second order model are also acceptable and fitted (Fig. 17 and Table 5). Moreover, the analysis of kinetics studies confirmed that the pseudo-first equation model could fit better than the pseudo-second order equation for the dye adsorption.[79,80]

### 3.5 Reusability study

Reusability is an important factor in the dye removal process to evaluate experimental uses with a cost-effective method. Fig. 18 shows the effect of reusability cycles on the removal of methylene blue, reactive orange GRN and cationic violet X-5BLN dyes and five successive adsorption cycles are observed. In the study, the recyclability of TP-SF/Fe for the degradation of dyes was determined in the presence of 0.1 g of TP-SF/Fe and 0.1 mmol L$^{-1}$ of $H_2O_2$ with a time of 30 min at pH 3, respectively. After every experimental run, the TP-SF/Fe was washed with deionized water and dried in a vacuum oven for repeated use. It was observed that the reusability cycle of TP-SF/Fe on dye removal for the 5th cycle was 98% for methylene blue, 79% for reactive orange GRN and 78% for cationic violet X-5BLN dyes. The reason may be that the small molecular products of dye degradation are adsorbed or complexed on the surface of TP-SF/Fe, which prevents them from

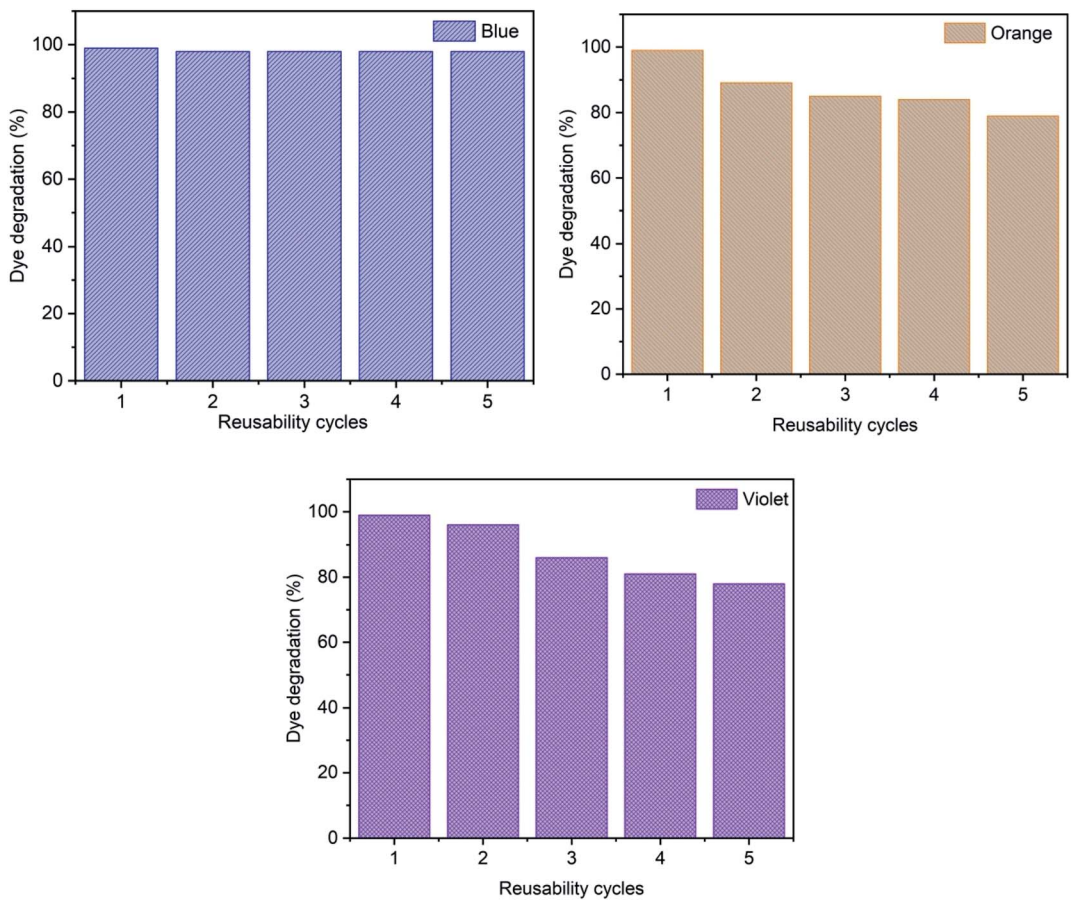


Fig. 18 Reusability analysis for the adsorption of methylene blue, reactive orange GRN, and cationic violet X-5BLN dyes.

Table 6 A comparison of adsorption capacities for methylene blue dyes using different adsorbents from previous research

| Adsorbent | $q_e$ (mg g$^{-1}$) | Reference |
|---|---|---|
| TP-SF/Fe | 13.09 | Present study |
| Orange peel | 5.87 | 7 |
| Titanate nanotubes (TNT24) | 5.644 | 15 |
| Polyethylene glycol 400 (Sn-PEG4) | 7.3 | 16 |
| Marine seaweed | 5.23 | 36 |
| $Cu_2O$ nanoparticles | 2.08 | 56 |
| Sawdust | 4.89 | 74 |
| Rice husk | 9.83 | 75 |
| Bamboo dust carbon | 9.66 | 79 |

catalyzing the decomposition of $H_2O_2$ to produce hydroxyl radicals. However, these results propose that the modified waste silk can be used for dye removal activities.

Furthermore, this research shows that the adsorption capacity of TP-SF/Fe for methylene blue is higher than many adsorbents explored in the literature. It may well be used in textile dye removal activities for its eco-friendliness, low-cost and satisfactory adsorption ability. The comparative results are listed in Table 6.

## 4. Conclusions

In this study, tea-phenol grafted waste silk fibers loaded with iron particles (TP-SF/Fe) were successfully used as an adsorbent for the efficient removal of methylene blue, reactive orange GRN, and cationic violet X-5BLN dyes from aqueous solution. The surface properties of TP-SF/Fe were investigated *via* FT-IR, SEM, EDS, and EDX analyses, which confirmed the successful loading of iron particles on the surface of TP-coated waste silk fibers. The TP-SF/Fe sample is a potential catalyst for the Fenton-like removal of aromatic dyes. The experimental results showed that pH is an important factor in the removal of dyes, and the maximum adsorption (99%) of dyes was achieved at 30 min. Moreover, the elevated results of the adsorption of dyes can be better explained based on the Freundlich adsorption isotherm model and pseudo-second order kinetics. The catalyst was reused five times for each dye. Therefore, waste silk can be used as a fiber-based catalyst for the Fenton-like removal of toxic pollutants from water.

## Conflicts of interest

The authors declare that they have no conflicts of interest with respect to the research, authorship, and/or publication of this article.

## Acknowledgements

This work was supported by the National Natural Science Foundation of China (51973144, 51741301), the Major Program of Natural Science Research of Jiangsu Higher Education Institutions of China (18KJA540002), and the Natural Science Foundation of Jiangsu Province (BK20201181).

## References

1 V. Gupta, A. Agarwal, M. K. Singh and N. B. Singh, Kail sawdust charcoal: a low-cost adsorbent for removal of textile dyes from aqueous solution, *SN Appl. Sci.*, 2019, **1**, 1271.
2 A. Ahmed, M. Usman, B. Yu, X. Ding, Q. Peng, Y. Shen and H. Cong, Efficient photocatalytic degradation of toxic Alizarin yellow R dye from industrial wastewater using biosynthesized Fe nanoparticle and study of factors affecting the degradation rate, *J. Photochem. Photobiol., B*, 2020, **202**, 111682.
3 A. Özverdi and M. Erdem, $Cu^{2+}$, $Cd^{2+}$ and $Pb^{2+}$ adsorption from aqueous solutions by pyrite and synthetic iron sulphide, *J. Hazard. Mater.*, 2006, **137**, 626–632.
4 M. T. Sulak and H. Cengiz Yatmaz, Removal of textile dyes from aqueous solutions with eco-friendly biosorbent, *Desalin. Water Treat.*, 2012, **37**, 169–177.
5 P. M. Gore, M. Naebe, X. Wang and B. Kandasubramanian, Progress in silk materials for integrated water treatments: Fabrication, modification and applications, *Chem. Eng. J.*, 2019, **374**, 437–470.
6 M. Naushad, A. A. Alqadami, A. A. A. Kahtani, T. Ahamad, M. R. Awual and T. Tatarchuk, Adsorption of textile dye using *para*-aminobenzoic acid modified activated carbon: Kinetic and equilibrium studies, *J. Mol. Liq.*, 2019, **296**, 112075.
7 D. Kavitha and C. Namasivayam, Experimental and kinetic studies on methylene blue adsorption by coir pith carbon, *Bioresour. Technol.*, 2007, **98**, 14–21.
8 E. Erdem, G. Çölgeçen and R. Donat, The removal of textile dyes by diatomite earth, *J. Colloid Interface Sci.*, 2005, **282**, 314–319.
9 A. P. Vieira, S. A. A. Santana, C. W. B. Bezerra, H. A. S. Silva, J. A. P. Chaves, J. C. P. Melo, E. C. S. Filho and C. Airoldi, Removal of textile dyes from aqueous solution by babassu coconut epicarp (Orbignya speciosa), *Chem. Eng. J.*, 2011, **173**, 334–340.
10 M. Atrous, L. Sellaoui, M. Bouzid, E. C. Lima, P. S. Thue, A. B. Petriciolet and A. B. Lamine, Adsorption of dyes acid red 1 and acid green 25 on grafted clay: Modeling and statistical physics interpretation, *J. Mol. Liq.*, 2019, **294**, 111610.
11 D. Bhatia, N. R. Sharma, J. Singh and R. S. Kanwar, Biological methods for textile dye removal from wastewater: A review, *Crit. Rev. Environ. Sci. Technol.*, 2017, **47**, 1836–1876.
12 T. H. Cheng, Z. J. Liu, J. Y. Yang, Y. Z. Huang, R. C. Tang and Y. F. Qiao, Extraction of functional dyes from tea stem waste in alkaline medium and their application for simultaneous coloration and flame retardant and bioactive functionalization of silk, *ACS Sustainable Chem. Eng.*, 2019, **7**, 18405–18413.
13 D. Rajkumar and J. G. Kim, Oxidation of various reactive dyes with *in situ* electro-generated active chlorine for textile dyeing industry wastewater treatment, *J. Hazard. Mater.*, 2006, **136**, 203–212.

14 I. F. Su, L. J. Chen and S. Y. Suen, Adsorption separation of terpene lactones from Ginkgo biloba L. extract using glass fiber membranes modified with octadecyltrichlorosilane, *J. Sep. Sci.*, 2005, **28**, 1211–1220.

15 M. N. Subramaniam, P. S. Goh, N. Abdullah, W. J. Lau, B. C. Ng and A. F. Ismail, Adsorption and photocatalytic degradation of methylene blue using high surface area titanate nanotubes (TNT) synthesized *via* hydrothermal method, *J. Nanopart. Res.*, 2017, **19**, 1–13.

16 B. Rani, S. Punniyakoti and N. K. Sahu, Polyol asserted hydrothermal synthesis of $SnO_2$ nanoparticles for the fast adsorption and photocatalytic degradation of methylene blue cationic dye, *New J. Chem.*, 2018, **42**, 943–954.

17 M. N. Morshed, N. Bouazizi, N. Behary, J. Guan and V. Nierstrasz, Stabilization of zero valent iron ($Fe^0$) on plasma/dendrimer functionalized polyester fabrics for Fenton-like removal of hazardous water pollutants, *Chem. Eng. J.*, 2019, **374**, 658–673.

18 P. A. Soares, T. F. C. V. Silva, D. R. Manenti, S. M. Souza, R. A. R. Boaventura and V. J. P. Vilar, Insights into real cotton-textile dyeing wastewater treatment using solar advanced oxidation processes, *Environ. Sci. Pollut. Res. Int.*, 2014, **21**, 932–945.

19 A. Alinsafi, F. Evenou, E. M. Abdulkarim, M. N. Pons, O. Zahraa, A. Benhammou, A. Yaacoubi and A. Nejmeddine, Treatment of textile industry wastewater by supported photocatalysis, *Dyes Pigm.*, 2007, **74**, 439–445.

20 N. Mohan, N. Balasubramanian and C. A. Basha, Electrochemical oxidation of textile wastewater and its reuse, *J. Hazard. Mater.*, 2007, **147**, 644–651.

21 F. Chen, A. S. Gong, M. Zhu, G. Chen, S. D. Lacey, F. Jiang, Y. Li, *et al.*, Mesoporous, three-dimensional wood membrane decorated with nanoparticles for highly efficient water treatment, *ACS Nano*, 2017, **11**, 4275–4282.

22 B. Merzouk, B. Gourich, A. Sekki, K. Madani, C. Vial and M. Barkaoui, Studies on the decolorization of textile dye wastewater by continuous electrocoagulation process, *Chem. Eng. J.*, 2009, **149**, 207–214.

23 P. Zhang, Q. Wang, J. Zhang, G. Li and Q. Wei, Preparation of amidoxime-modified polyacrylonitrile nanofibers immobilized with laccase for dye degradation, *Fibers Polym.*, 2014, **15**, 30–34.

24 Y. Zhang, X. Fan, Q. Wang and A. C. Paulo, Preparation of functionalized cotton based on laccase-catalyzed synthesis of polyaniline in perfluorooctanesulfonate acid potassium salt (PFOS) template, *RSC Adv.*, 2016, **6**, 49272–49280.

25 A. Khalid, M. Arshad and D. E. Crowley, Biodegradation potential of pure and mixed bacterial cultures for removal of 4-nitroaniline from textile dye wastewater, *Water Res.*, 2009, **43**, 1110–1116.

26 C. Wu, T. W. Kim, F. Li and T. Guo, Wearable electricity generators fabricated utilizing transparent electronic textiles based on polyester/Ag nanowires/graphene core–shell nanocomposites, *ACS Nano*, 2016, **10**, 6449–6457.

27 Y. Jiao, C. Wan, W. Bao, H. Gao, D. Liang and J. Li, Facile hydrothermal synthesis of $Fe_3O_4$@cellulose aerogel nanocomposite and its application in Fenton-like degradation of Rhodamine B, *Carbohydr. Polym.*, 2018, **189**, 371–378.

28 Q. C. Do, D. G. Kim and S. Ko, Nonsacrificial template synthesis of magnetic-based yolk–shell nanostructures for the removal of acetaminophen in Fenton-like systems, *ACS Appl. Mater. Interfaces*, 2017, **9**, 28508–28518.

29 C. L. Hsueh, Y. H. Huang, C. C. Wang and C. Y. Chen, Degradation of azo dyes using low iron concentration of Fenton and Fenton-like system, *Chemosphere*, 2005, **58**, 1409–1414.

30 C. Bouasla, M. E. H. Samar and F. Ismail, Degradation of methyl violet 6B dye by the Fenton process, *Desalination*, 2010, **254**, 35–41.

31 R. Aplin and T. D. Waite, Comparison of three advanced oxidation processes for degradation of textile dyes, *Water Sci. Technol.*, 2000, **42**, 345–354.

32 K. Ntampegliotis, A. Riga, V. Karayannis, V. Bontozoglou and G. Papapolymerou, Decolorization kinetics of Procion H-exl dyes from textile dyeing using Fenton-like reactions, *J. Hazard. Mater.*, 2006, **136**, 75–84.

33 M. Sökmen and A. Özkan, Decolourising textile wastewater with modified titania: the effects of inorganic anions on the photocatalysis, *J. Photochem. Photobiol., A*, 2002, **147**, 77–81.

34 M. Dindarsafa, A. Khataee, B. Kaymak, B. Vahid, A. Karimi and A. Rahmani, Heterogeneous sono-Fenton-like process using martite nanocatalyst prepared by high energy planetary ball milling for treatment of a textile dye, *Ultrason. Sonochem.*, 2017, **34**, 389–399.

35 P. B. Koli, K. H. Kapadnis and U. G. Deshpande, Transition metal decorated Ferrosoferric oxide ($Fe_3O_4$): An expeditious catalyst for photodegradation of Carbol Fuchsin in environmental remediation, *J. Environ. Chem. Eng.*, 2019, **7**, 103373.

36 S. Cengiz and L. Cavas, Removal of methylene blue by invasive marine seaweed: Caulerpa racemosa var. cylindracea, *Bioresour. Technol.*, 2008, **99**, 2357–2363.

37 M. S. Mia, B. Yan, X. Zhu, T. Xing and G. Chen, Dopamine Grafted Iron-Loaded Waste Silk for Fenton-Like Removal of Toxic Water Pollutants, *Polymers*, 2019, **11**, 2037.

38 Q. Zhou, W. Wu, S. Zhou, T. Xing, G. Sun and G. Chen, Polydopamine-induced growth of mineralized γ-FeOOH nanorods for construction of silk fabric with excellent superhydrophobicity, flame retardancy and UV resistance, *Chem. Eng. J.*, 2020, **382**, 122988.

39 C. Holland, K. Numata, J. R. Kovacina and F. P. Seib, The biomedical use of silk: past, present, future, *Adv. Healthcare Mater.*, 2019, **8**, 1800465.

40 S. Chen, L. Cheng, H. Huang, F. Zou and H. P. Zhao, Fabrication and properties of poly (butylene succinate) biocomposites reinforced by waste silkworm silk fabric, *Composites, Part A*, 2017, **95**, 125–131.

41 M. Ho, K. Lau, H. Wang and D. Bhattacharyya, Characteristics of a silk fibre reinforced biodegradable plastic, *Composites, Part B*, 2011, **42**, 117–122.

42 Q. T. H. Shubhra, A. K. M. M. Alam, M. A. Khan, M. Saha, D. Saha and M. A. Gafur, Study on the mechanical

properties, environmental effect, degradation characteristics and ionizing radiation effect on silk reinforced polypropylene/natural rubber composites, *Composites, Part A*, 2010, **41**, 1587–1596.

43 X. Zhu, B. Yan, X. Yan, T. Wei, H. Yao, M. S. Mia, T. Xing and G. Chen, Fabrication of non-iridescent structural color on silk surface by rapid polymerization of dopamine, *Prog. Org. Coat.*, 2020, **149**, 105904.

44 A. Bhatnagar, W. Hogland, M. Marques and M. Sillanpää, An overview of the modification methods of activated carbon for its water treatment applications, *Chem. Eng. J.*, 2013, **219**, 499–511.

45 C. S. Yang, J. Y. Chung, G. Yang, S. K. Chhabra and M. J. Lee, Tea and tea polyphenols in cancer prevention, *J. Nutr.*, 2000, **130**, 472S–478S.

46 T. Ozdal, E. Capanoglu and F. Altay, A review on protein–phenolic interactions and associated changes, *Int. Food Res. J.*, 2013, **51**, 954–970.

47 T. P. Kondratyuk and J. M. Pezzuto, Natural product polyphenols of relevance to human health, *Pharm. Biol.*, 2004, **42**, 46–63.

48 G. E. Hoag, J. B. Collins, J. L. Holcomb, J. R. Hoag, M. N. Nadagouda and R. S. Varma, Degradation of bromothymol blue by 'greener'nano-scale zero-valent iron synthesized using tea polyphenols, *J. Mater. Chem.*, 2009, **19**, 8671–8677.

49 M. Zou, M. L. Du, H. Zhu, C. S. Xu, N. Li and Y. Q. Fu, Synthesis of silver nanoparticles in electrospun polyacrylonitrile nanofibers using tea polyphenols as the reductant, *Polym. Eng. Sci.*, 2013, **53**, 1099–1108.

50 B. Yan, Q. Zhou, X. Zhu, J. Guo, M. S. Mia, X. Yan, G. Chen and T. Xing, A superhydrophobic bionic coating on silk fabric with flame retardancy and UV shielding ability, *Appl. Surf. Sci.*, 2019, **483**, 929–939.

51 T. H. Cheng, Z. J. Liu, J. Y. Yang, Y. Z. Huang, R. C. Tang and Y. F. Qiao, Extraction of functional dyes from tea stem waste in alkaline medium and their application for simultaneous coloration and flame retardant and bioactive functionalization of silk, *ACS Sustainable Chem. Eng.*, 2019, **7**, 18405–18413.

52 H. Pang, S. Zhao, L. Mo, Z. Wang, W. Zhang, A. Huang, S. Zhang and J. Li, Mussel-inspired bio-based water-resistant soy adhesives with low-cost dopamine analogue-modified silkworm silk Fiber, *J. Appl. Polym. Sci.*, 2020, **137**, 48785.

53 B. Yan, Q. Zhou, X. Zhu, J. Guo, Md S. Mia, X. Yan, G. Chen and T. Xing*, A superhydrophobic bionic coating on silk fabric with flame retardancy and UV shielding ability, *Appl. Surf. Sci.*, 2019, **483**, 929–939.

54 L. Huang, X. Weng, Z. Chen, M. Megharaj and R. Naidu, Green synthesis of iron nanoparticles by various tea extracts: comparative study of the reactivity, *Spectrochim. Acta, Part A*, 2014, **130**, 295–301.

55 J. He, W. Ma, J. He, J. Zhao and C. Y. Jimmy, Photooxidation of azo dye in aqueous dispersions of $H_2O_2$/α-FeOOH, *Appl. Catal., B*, 2002, **39**, 211–220.

56 K. V. Mrunal, A. K. Vishnu, N. Momin and J. Manjanna, $Cu_2O$ nanoparticles for adsorption and photocatalytic degradation of methylene blue dye from aqueous medium, *Environ. Nanotechnol. Monit. Manage.*, 2019, **12**, 100265.

57 H. Pang, S. Zhao, L. Mo, Z. Wang, W. Zhang, A. Huang, S. Zhang and J. Li, Mussel-inspired bio-based water-resistant soy adhesives with low-cost dopamine analogue-modified silkworm silk Fiber, *J. Appl. Polym. Sci.*, 2020, **137**, 48785.

58 D. Solomon, J. Lehmann, J. Harden, J. Wang, J. Kinyangi, K. Heymann, C. Karunakaran, Y. Lu, S. Wirick and C. Jacobsen, Micro-and nano-environments of carbon sequestration: Multi-element STXM–NEXAFS spectromicroscopy assessment of microbial carbon and mineral associations, *Chem. Geol.*, 2012, **329**, 53–73.

59 A. Majumdar, J. Schäfer, P. Mishra, D. Ghose, J. Meichsner and R. Hippler, Chemical composition and bond structure of carbon-nitride films deposited by $CH_4/N_2$ dielectric barrier discharge, *Surf. Coat. Technol.*, 2007, **201**, 6437–6444.

60 P. Singh, A. Sarswat, C. U. Pittman Jr, T. Mlsna and D. Mohan, Sustainable Low-Concentration Arsenite [As(III)] Removal in Single and Multicomponent Systems Using Hybrid Iron Oxide–Biochar Nanocomposite Adsorbents—A Mechanistic Study, *ACS Omega*, 2020, **5**, 2575–2593.

61 D. J. Jing, Y. P. Yuan, J. X. Sun, F. M. Peng, X. Jiang, L. G. Qiu, A. J. Xie, Y. H. Shen and J. F. Zhu, New photocatalysts based on MIL-53 metal–organic frameworks for the decolorization of methylene blue dye, *J. Hazard. Mater.*, 2011, **190**, 945–951.

62 P. K. Priyanka, S. Tambat, S. Sontakke and P. Nemade, Visible light removal of reactive dyes using $CeO_2$ synthesized by precipitation, *J. Environ. Chem. Eng.*, 2018, **6**, 4476–4489.

63 B. K. Nandi, A. Goswami and M. K. Purkait, Removal of cationic dyes from aqueous solutions by kaolin: kinetic and equilibrium studies, *Appl. Clay Sci.*, 2009, **42**, 583–590.

64 J. S. Wu, C. H. Liu, K. H. Chu and S. Y. Suen, Removal of cationic dye methyl violet 2B from water by cation exchange membranes, *J. Membr. Sci.*, 2008, **309**, 239–245.

65 R. Sivaraj, R. Venckatesh and S. G. Gowri, Activated carbon prepared from Eichornia crassipes as an adsorbent for the removal of dyes from aqueous solution, *Int. J. Eng. Sci. Technol.*, 2010, **2**, 2418–2427.

66 M. Neamtu, I. Siminiceanu, A. Yediler and A. Kettrup, Kinetics of decolorization and mineralization of reactive azo dyes in aqueous solution by the UV/$H_2O_2$ oxidation, *Dyes Pigm.*, 2002, **53**, 93–99.

67 M. Neamţu, C. Catrinescu and A. Kettrup, Effect of dealumination of iron (III)—exchanged Y zeolites on oxidation of Reactive Yellow 84 azo dye in the presence of hydrogen peroxide, *Appl. Catal., B*, 2004, **51**, 149–157.

68 J. L. Gong, B. Wang, G. M. Zeng, C. P. Yang, C. G. Niu, Q. Y. Niu, W. J. Zhou and Y. Liang, Removal of cationic dyes from aqueous solution using magnetic multi-wall carbon nanotube nanocomposite as adsorbent, *J. Hazard. Mater.*, 2009, **164**, 1517–1522.

69 N. Bouanimba, R. Zouaghi, N. Laid and T. Sehili, Factors influencing the photocatalytic decolorization of

Bromophenol blue in aqueous solution with different types of $TiO_2$ as photocatalysts, *Desalination*, 2011, **275**, 224–230.

70 S. Rashid, C. Shen, J. Yang, J. Liu and J. Li, Preparation and properties of chitosan–metal complex: some factors influencing the adsorption capacity for dyes in aqueous solution, *J. Environ. Sci.*, 2018, **66**, 301–309.

71 M. D. G. de Luna, E. D. Flores, D. A. D. Genuino, C. M. Futalan and M. W. Wan, Adsorption of Eriochrome Black T (EBT) dye using activated carbon prepared from waste rice hulls—Optimization, isotherm and kinetic studies, *J. Taiwan Inst. Chem. Eng.*, 2013, **44**, 646–653.

72 S. Xiao, Z. Wang, H. Ma, H. Yang and W. Xu, Effective removal of dyes from aqueous solution using ultrafine silk fibroin powder, *Adv. Powder Technol.*, 2014, **25**, 574–581.

73 M. Ghasemi, M. Naushad, N. Ghasemi and Y. K. Fard, Adsorption of Pb(II) from aqueous solution using new adsorbents prepared from agricultural waste: adsorption isotherm and kinetic studies, *J. Ind. Eng. Chem.*, 2014, **20**, 2193–2199.

74 I. Uzun and F. Güzel, Kinetics and thermodynamics of the adsorption of some dyestuffs and *p*-nitrophenol by chitosan and MCM-chitosan from aqueous solution, *J. Colloid Interface Sci.*, 2004, **274**, 398–412.

75 C. Y. Sharma, Optimization of parameters for adsorption of methylene blue on a low-cost activated carbon, *J. Chem. Eng. Data*, 2010, **55**, 435–439.

76 I. A. W. Tan, A. L. Ahmad and B. H. Hameed, Adsorption of basic dye on high-surface-area activated carbon prepared from coconut husk: Equilibrium, kinetic and thermodynamic studies, *J. Hazard. Mater.*, 2008, **154**, 337–346.

77 G. Vijayakumar, R. Tamilarasan and M. Dharmendirakumar, Adsorption, Kinetic, Equilibrium and Thermodynamic studies on the removal of basic dye Rhodamine-B from aqueous solution by the use of natural adsorbent perlite, *J. Mater. Environ. Sci.*, 2012, **3**, 157–170.

78 J. Rahchamani, H. Z. Mousavi and M. Behzad, Adsorption of methyl violet from aqueous solution by polyacrylamide as an adsorbent: Isotherm and kinetic studies, *Desalination*, 2011, **267**, 256–260.

79 N. Kannan and M. M. Sundaram, Kinetics and mechanism of removal of methylene blue by adsorption on various carbons—a comparative study, *Dyes Pigm.*, 2001, **51**, 25–40.

80 B. H. Hameed, D. K. Mahmoud and A. L. Ahmad, Equilibrium modeling and kinetic studies on the adsorption of basic dye by a low-cost adsorbent: Coconut (Cocos nucifera) bunch waste, *J. Hazard. Mater.*, 2008, **158**, 65–72.